Signs of interacting vacuum and dark matter in the universe

Joan Solà Peracaula*, Adrià Gómez-Valent and Javier de Cruz Pérez

Departament de Física Quàntica i Astrofísica (FQA),
and Institute of Cosmos Sciences (ICCUB)
Universitat de Barcelona, Av. Diagonal 647, E-08028 Barcelona, Catalonia, Spain
sola@fqa.ub.edu, adriagova@fqa.ub.edu, decruz@fqa.ub.edu

We consider the impact of dynamical dark energy (DDE) in the possible solution of the existing tensions in the ΛCDM. We test both interacting and non-interacting DE models with dark matter (DM). Among the former, the running vacuum model (RVM) interacting with DM appears as a favored option. The non-interacting scalar field model based on the potential $V \sim \phi^{-\alpha}$, and the generic XCDM parametrization, also provide consistent signs of DDE. The important novelty of our analysis with respect to the existing ones in the literature is that we use the matter bispectrum, together with the power spectrum. Using a complete and updated set of cosmological observations on SNIa+BAO+$H(z)$+LSS+CMB, we find that the crucial triad BAO+LSS+CMB (i.e. baryonic acoustic oscillations, large scale structure formation data and the cosmic microwave background) provide the bulk of the signal. The bispectrum data is instrumental to get hold of the DDE signal, as our analysis shows. If the bispectrum is not included, the DDE signal could not be currently perceived at a significant confidence level.

Keywords: Cosmological constant; dark energy theory; cosmological parameters; structure formation; cosmic microwave background.

1. Introduction

The cosmological constant problem in the context of quantum field theory (QFT) is well known. Already in the standard model of particle physics the value of the vacuum energy density ρ_Λ is predicted to be some 55 orders of magnitude higher than the measured value, $\rho_\Lambda \sim 10^{-47}$ GeV^4 see Refs. 1–5. Rather than attempting to solve this problem here, we adopt a pragmatic point of view and consider the possibility to test whether the vacuum energy, and in general the dark energy (DE), is dynamical or not in the light of the current observations. This might help to shed some light not only on how to cure the CC-problem eventually, but also on how to solve some of the existing tensions between the ΛCDM model and observations, like the H_0-tension (the mismatch between the Planck measurements of H_0 and the local measurements based on the distance ladder approach)[6–8] and the σ_8-tension, which is described in terms of the combined observable $f(z)\sigma_8(z)$, where $f(z)$ is the linear growth rate and $\sigma_8(z)$ is the RMS matter fluctuation on scales of $R_8 = 8h^{-1}$ Mpc at redshift z. The corresponding prediction of the ΛCDM is known to be exceedingly large and hence the description of the LSS data is poorly accounted for by the concordance model.[9,10] In the following we briefly review how dynamical dark energy (DDE) can lend a helping hand on trying to solve some of these problems, although the evidence of DDE (or lack of it) varies significantly if taking different
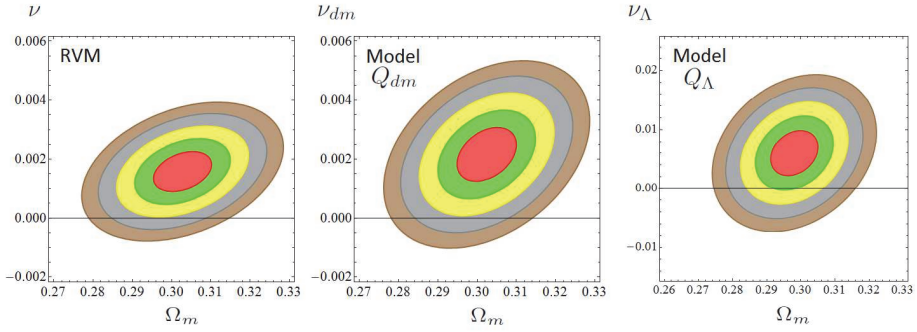
---

*Speaker

Fig. 1. Likelihood contours for the three DVMs (3)-(5) in the (Ω_m, ν_i) plane up to 5σ c.l. after marginalizing over the rest of the fitting parameters. Use is made of SNIa+BAO+$H(z)$+LSS data and compressed CMB Planck 2015 data. The ΛCDM ($\nu_i = 0$) appears disfavored in front of the DVMs. In particular, the RVM and the Q_{dm} are favored at $\sim 3\sigma$ c.l. See Ref. 14 for details on the SNIa+BAO+$H(z)$+LSS+CMB data used in our fit. We note, in particular, that bispectrum data is also included.[20]

studies in the literature, see Refs. 11–17 and the more recent analyses 18, 19 and references therein.

2. Cosmology beyond $\Lambda = $ const.

The Friedmann and acceleration equations when the vacuum evolves with the cosmic expansion, $\rho_\Lambda = \rho_\Lambda(t)$ can be written formally similar to the standard case when $\rho_\Lambda =$const. If we focus on flat FLRW metric, the field equations that incorporate vacuum dynamics read

$$3H^2 = 8\pi G(\rho_m + \rho_\Lambda(t)), \qquad 2\dot{H} + 3H^2 = -8\pi G(w_m \rho_m + w_\Lambda \rho_\Lambda(t)), \qquad (1)$$

where $w_m = 1/3, 0$ for relativistic and nonrelativistic matter, and $w_\Lambda = -1$ for the vacuum (irrespective of its time evolution). Hereafter we assume $w_\Lambda = -1$ – see 12 for the analysis of the general case with $w_\Lambda = -1 + \epsilon$ ($|\epsilon| \ll 1$), i.e. for quasivacuum models. The total matter density ρ_m involves the contributions from baryons and cold dark matter (DM): $\rho_m = \rho_b + \rho_{dm}$. We assume that the DM component is the only one that interacts with vacuum, whilst radiation and baryons are taken to be self-conserved, hence $\rho_r(a) = \rho_r^0 a^{-4}$ and $\rho_b(a) = \rho_b^0 a^{-3}$, where the superscript zero denotes the current values. The DM component, instead, exchanges energy with the vacuum, and the local conservation law reads

$$\dot{\rho}_{dm} + 3H\rho_{dm} = Q, \qquad \dot{\rho}_\Lambda = -Q. \qquad (2)$$

The form of the source function Q depends on the assumptions made on the dynamical vacuum model (DVM). Let us consider three model possibilities, one is the "running vacuum model" (RVM) — see Refs. 3–5. and references therein — and the other two are called the Q_{dm} and Q_Λ models, whose names bear relation to the

structure of the interaction source. For convenience they can also be labeled I, II and III:

$$\text{Model I \ (RVM)} : \ Q = \nu\, H(3\rho_m + 4\rho_r) \tag{3}$$

$$\text{Model II \ } (Q_{dm}) : \ Q_{dm} = 3\nu_{dm}H\rho_{dm} \tag{4}$$

$$\text{Model III \ } (Q_\Lambda) : \ Q_\Lambda = 3\nu_\Lambda H\rho_\Lambda \,. \tag{5}$$

Each model is characterized by a (dimensionless) coupling parameter $\nu_i = \nu, \nu_{dm}, \nu_\Lambda$ in the interaction source, to be fitted to the observational data. In the RVM case, the source function Q in (3) can be derived from the following vacuum energy density:

$$\rho_\Lambda(H) = \frac{3}{8\pi G}\left(c_0 + \nu H^2\right) , \tag{6}$$

which can be motivated in QFT, see Ref. 3.[a] The other two models do not possess an analogous property and therefore are more *ad hoc*. The additive constant c_0 in (6) is fixed by the boundary condition $\rho_\Lambda(H = H_0) = \rho_\Lambda^0$, where H_0 is the current Hubble rate and ρ_Λ^0 is the present measured value for ρ_Λ. The dimensionless parameter ν encodes the dynamics of the vacuum and can be related with the β-function of the ρ_Λ-running.[3] Therefore we naturally expect $|\nu| << 1$ in QFT. Here we will treat ν as a free parameter of the RVM and, as indicated, it will be fitted to the data.

In Fig. 1 we display the fitting results on the (Ω_m, ν_i)-planes for the three models I, II and III (corresponding to $\nu_i = \nu, \nu_{dm}, \nu_\Lambda$), where Ω_m is the usual matter parameter at present. In Fig. 2 we can better appraise the impact of the various data sources on these contour plots in the specific case of the RVM, see Ref. 14 for details. The DDE option ($\nu \neq 0$, actually $\nu > 0$) is clearly favored in the last plot when we combine the crucial triad of BAO+LSS+CMB data.

3. Analytical solution of the dynamical vacuum models

One can solve Models I, II and III analytically in terms of the scale factor.[14] The DM density in the case of the RVM (Model I) as a function of the scale factor is

$$\rho_{dm}^{(I)} = \rho_{dm}^0\, a^{-3(1-\nu)} + \rho_b^0\left(a^{-3(1-\nu)} - a^{-3}\right) - \frac{4\nu\rho_r^0}{1+3\nu}\left(a^{-4} - a^{-3(1-\nu)}\right) \tag{7}$$

and that of the vacuum energy density reads

$$\rho_\Lambda^{(I)} = \rho_\Lambda^0 + \frac{\nu}{1-\nu}\left[\rho_m^0\left(a^{-3(1-\nu)} - 1\right) + \rho_r^0\left(\frac{(1-\nu)\,a^{-4} + 4\nu a^{-3(1-\nu)}}{1+3\nu} - 1\right)\right]. \tag{8}$$

The total matter density is just the sum of the conserved baryonic and radiation densities and the above DM density. As can be easily checked, for $\nu \to 0$ we recover the corresponding results for the ΛCDM, as it should.

---

[a]The structure of the vacuum energy density in the running vacuum model can also be motivated from the effective behavior of the power-law solutions of Brans-Dicke gravity, see Ref. 21.
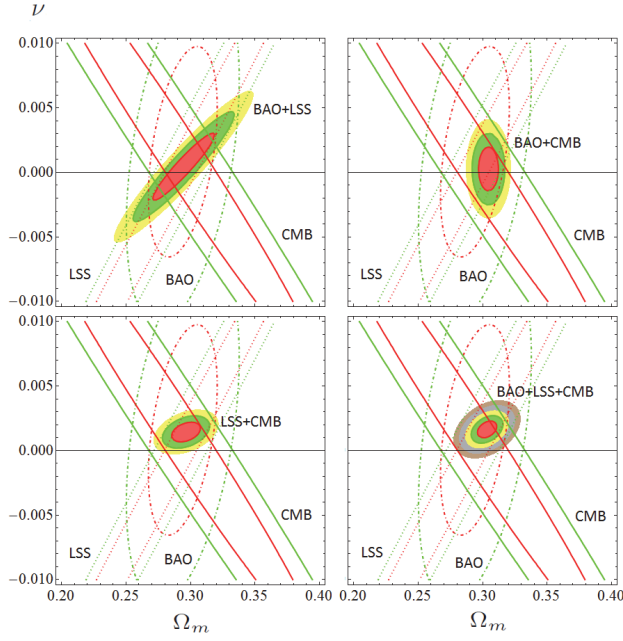
Fig. 2. Contour lines for the RVM by considering the effect of only BAO, LSS and CMB in all the possible pairings. Same data as in Fig. 1. Remarkably the simultaneous combination of these three observables is able to capture signs of running vacuum at a confidence level of $\gtrsim 3\sigma$.

For Model II:

$$\rho_{dm}^{(II)}(a) = \rho_{dm}^0 \, a^{-3(1-\nu_{dm})} \tag{9}$$

and

$$\rho_{\Lambda}^{(II)}(a) = \rho_{\Lambda}^0 + \frac{\nu_{dm} \, \rho_{dm}^0}{1-\nu_{dm}} \left(a^{-3(1-\nu_{dm})} - 1 \right) . \tag{10}$$

And for Model III:

$$\rho_{dm}^{(III)}(a) = \rho_{dm}^0 \, a^{-3} + \frac{\nu_{\Lambda}}{1-\nu_{\Lambda}} \rho_{\Lambda}^0 \left(a^{-3\nu_{\Lambda}} - a^{-3} \right) \tag{11}$$

and

$$\rho_{\Lambda}^{(III)}(a) = \rho_{\Lambda}^0 \, a^{-3\nu_{\Lambda}} . \tag{12}$$

Let us also briefly consider the simplest parametrization for DDE, namely the XCDM,[22] in which the DE density as a function of the scale factor is simply given by $\rho_X(a) = \rho_{X0} \, a^{-3(1+w_0)}$, with $\rho_{X0} = \rho_{\Lambda 0}$. Here w_0 is the (constant) EoS parameter. Last, but not least, we also study a scalar field model, denoted as ϕCDM. In this type of models the DE has a well-defined local Lagrangian description in terms

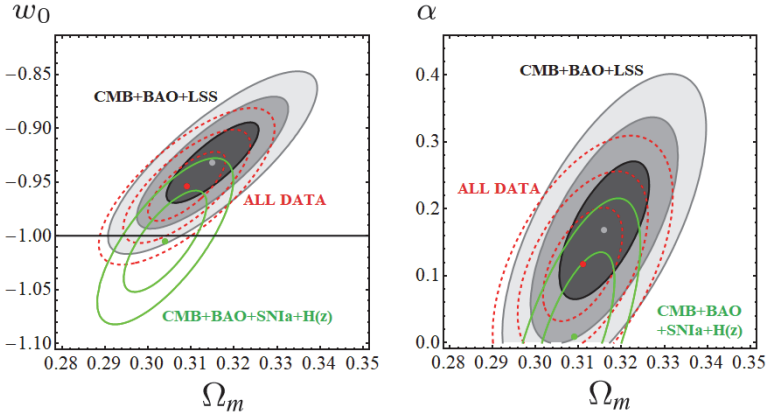Fig. 3. Contour plots for the XCDM parametrization (left) and ϕCDM (right), using all sources of data (including LSS with bispectrum) as compared to using all data except LSS. Here we use Planck 2018 data with compressed CMB likelihood. When LSS (with bispectrum) is included, DDE appears once more favored at $\sim 3\sigma$ c.l. See Ref. 18 for details.

of a scalar field. Taking ϕ dimensionless the energy density and pressure read

$$\rho_\phi = \frac{M_P^2}{16\pi}\left(\frac{\dot{\phi}^2}{2} + V(\phi)\right) \qquad p_\phi = \frac{M_P^2}{16\pi}\left(\frac{\dot{\phi}^2}{2} - V(\phi)\right), \qquad (13)$$

where M_P is the Planck mass, which in natural units takes the value $M_P = 1/\sqrt{G}$ $= 1.2211 \times 10^{19}$ GeV. Note that in our conventions $V(\phi)$ has dimension 2 in natural units. The scalar field satisfies the Klein-Gordon equation in the context of the FLRW metric $\ddot{\phi} + 3H\dot{\phi} + \partial V(\phi)/\partial\phi = 0$. Here, as a particular case, we consider the original quintessence potential by Peebles and Ratra:[23]

$$V(\phi) = \frac{1}{2}\kappa M_P^2 \phi^{-\alpha}, \qquad (14)$$

where κ and α are dimensionless. The parameter α should be positive and sufficiently small so that $V(\phi)$ can mimic approximately a CC slowly decreasing with time, such that it can eventually surface (near our time) over the rapidly decaying matter density. In Fig. 3 we can see the corresponding contour lines for both the XCDM and ϕCDM, using SNIa+BAO+$H(z)$+LSS data (including the bispectrum component for the LSS+BAO data from Ref. 20) and compressed CMB Planck 2018 likelihood. The DDE option is consistently favored in both cases since $w_0 > -1$ (for the XCDM) and $\alpha > 0$ (for the ϕCDM) at $\lesssim 3\sigma$ c.l. after marginalizing over Ω_m [b]. Failure of including the bispectrum component (which seems to be particularly sensitive to the dynamics of the DE) may explain why other recent analyses on interacting vacuum and ϕCDM could not trace signs of DDE, see e.g., Refs. 16, 17.

---

[b]We should point out that a similar level of evidence is obtained using Planck 2015 data with full (i.e. non-compressed) CMB likelihood, see Ref. 18 for details.
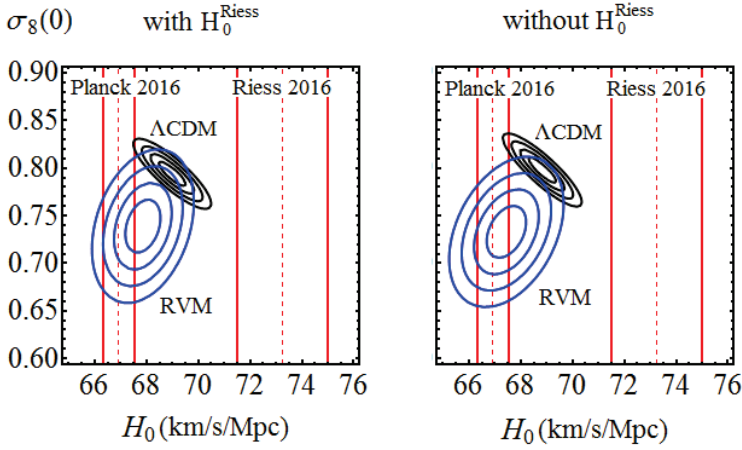
Fig. 4.   Contour lines for the ΛCDM (black) and RVM (blue) up to 4σ in the $(H_0, \sigma_8(0))$-plane [12]. On the left plot we have included the R16 point [8] on H_0 in our fit, whereas on the right plot it was not included. In both cases the favored range for H_0 is the Planck range. At the same time the optimal (lower) $\sigma_8(0)$ values are attained by the RVM, see Eq. (3), whereas the ΛCDM yields too large values.

4. Dealing with the tensions through vacuum dynamics

As indicated in the introduction, one of the persisting tensions with the ΛCDM is the discrepancy between the Planck value of the Hubble parameter H_0 obtained from the CMB anisotropies, and the local HST measurement (based on distance ladder estimates from Cepheids). The latter reads $H_0 = 73.24 \pm 1.74$ km/s/Mpc (referred to as R16) and $H_0 = 73.48 \pm 1.66$ km/s/Mpc (R18). [8] In contrast, the CMB value is $H_0 = 67.51 \pm 0.64$ km/s/Mpc, as extracted from Planck 2015 TT,TE,EE+lowP+lensing data, or $H_0 = 66.93 \pm 0.62$ km/s/Mpc, based on Planck 2015 TT,TE,EE+SIMlow data. [6] In both cases there is a tension above 3σ c.l. with respect to the local measurement. This controversial situation has stimulated a lot of discussion in the literature. For instance, in Ref. 24 the phantom DE option is exploited as a means to solve the tension. In contrast, in Ref. 12 it is proposed that vacuum and quasivacuum dynamics support the Planck measurement of H_0 against the local measurement with no need of phantom behavior. A similar conclusion is reached with the XCDM and ϕCDM models studied here. [18] In addition, a variety of model-independent approaches such as the Inverse Distance Ladder method or the Multi-Task Gaussian Process [25] as well as other techniques (e.g., the Weighted Polynomial Regression [26]) do also support a lower value of H_0 in the ballpark of Planck CMB measurements and hence in full consistency with DDE.

The H_0-tension is closely connected with another type of problem, which is the role played by the LSS data, namely the data on $f(z)\sigma_8(z)$. There seems to be no way at present to correctly account for both the CMB and the LSS data within

the ΛCDM. This new pitfall is at the root of the so-called σ_8-tension, one of the most intriguing phenomenological problems of the ΛCDM.[9,10] The problem has been dealt with in the literature from a variety of points of view, see e.g., Refs. 27, 28. Here we will focus once more on the possibility of DDE.[12–14,18]

In the presence of interacting vacuum the perturbations equations of the ΛCDM must be modified appropriately.[13,14] The detailed analysis of these matters performed in the mentioned references provides the basis for a possible solution to the σ_8-tension within the RVM. In Fig. 4, we present the likelihood contours in the $(H_0, \sigma_8(0))$-plane. In the left plot we show the situation when the local H_0 value R16 is included in the fit, whereas in the right plot we show the case when that local value is *not* included. The plots for the more updated R18 value would be almost indistinguishable from the R16 ones. From Fig. 4 we can see that in order to reach the R16 neighborhood the contours should be extended beyond the 5σ c.l., which would lead to a too large value of $\sigma_8(0)$ for the RVM. One can also show that it would lead to a too low value of Ω_m.[12]

Notice that H_0 and $\sigma_8(0)$ are positively correlated in the RVM (i.e. H_0 increases/decreases when $\sigma_8(0)$ increases/decreases, respectively), whilst they are anticorrelated in the ΛCDM (H_0 increases when $\sigma_8(0)$ decreases, and vice versa). The simultaneous H_0 and $\sigma_8(0)$ tensions could only be resolved simultaneously if the contours are extended well beyond 5σ at the expense of values of Ω_m below 0.27. However, this does not seem to be the most likely solution. Vacuum dynamics offers a better scenario. The opposite correlation feature with respect to the ΛCDM allows e.g., the RVM to improve the LSS fit in the region where both H_0 and $\sigma_8(0)$ are smaller than the respective ΛCDM values (cf. Fig. 4). This explains why the Planck range for H_0 is clearly preferred by the RVM, as it allows a much better description of the LSS data. One can also derive similar conclusions using the XCDM and ϕCDM, see Ref. 18, where again a positive correlation between H_0 and $\sigma_8(0)$ is found and the LSS tension can then be relaxed in the range of Planck values of H_0.

5. Conclusions

We have analyzed the ability of dynamical dark energy (DDE) models to fit the overall cosmological observations as compared to the ΛCDM. We find that there is non-negligible evidence that these models are more favored. Furthermore, DDE is capable of smoothing out the LSS tensions of the concordance model with the data, and they favor the (lower) Planck value of H_0 over the local one.

Acknowledgments

References

1. S. Weinberg, Rev. of Mod. Phys. **61** (1989) 1.
2. P.J.E. Peebles & B. Ratra, Rev. Mod. Phys. **75** (2003) 559.
3. J. Solà, J. Phys. Conf. Ser. **453** (2013) 012015; AIP Conf.Proc. **1606** (2014) 19.
4. J. Solà & A. Gómez-Valent, Int. J. Mod. Phys. D**24** (2015) 1541003.
5. A. Gómez-Valent, PhD Thesis, arXiv:1710.01978.
6. Planck 2015 results: P.A.R Ade *et al.*, A&A **594** (2016) A13: Planck 2016 intermediate results: N. Aghanim *et al.*, A&A **596** (2016) A107.
7. Planck 2018 results: N. Aghanim *et al.*, arXiv:1807.06209.
8. A.G. Riess *et al.*, ApJ. **826** (2016) 56; A.G. Riess *et al.*, ApJ. **855** (2018) 136.
9. E. Macaulay, I.K. Wehus I.K. & H.C. Eriksen, Phys. Rev. Lett. **111** (2013) 161301.
10. S. Basilakos & S. Nesseris, Phys. Rev. D**96** (2017) 063517.
11. J. Solà, A. Gómez-Valent & J. de Cruz Pérez, ApJ **811** (2015) L14; ApJ. **836** (2017) 43; Mod. Phys. Lett. A**32** (2017) 1750054.
12. J. Solà, A. Gómez-Valent & J. de Cruz Pérez, Phys. Lett. B**774** (2017) 317; Int. J. Mod. Phys. A**32** (2017) 1730014.
13. A. Gómez-Valent & J. Solà, MNRAS **478** (2018) 126; EPL 120 (2017) 39001.
14. J. Solà, J. de Cruz Pérez & A. Gómez-Valent, MNRAS **478** (2018) 4357; EPL **121** (2018) 39001.
15. G.B. Zhao *et al.*, Nat. Astron. **1** (2017) 627.
16. A.A. Costa *et al.*, JCAP **1701** (2017) 028; Y.H. Li *et al.* Phys. Rev. D**93** (2016) 023002; Phys. Rev. D**90** (2014) 123007; Phys. Rev. D90 (2014) 063005.
17. C-G. Park & B. Ratra, ApJ **868** (2018) 83; arXiv:1803.05522; J. Ooba, B. Ratra & N. Sugiyama, arXiv:1802.05571.
18. J. Solà, A. Gómez-Valent & J. de Cruz Pérez, "Signs of Dynamical Dark Energy in Current Observations", arXiv:1811.03505 (to appear in Phys. Dark Univ., 2019).
19. M. Martinelli, N.B. Hogg, S. Peirone, M. Bruni & D. Wands, arXiv:1902.10694.
20. H. Gil-Marín *et al.*, MNRAS **465** (2017) 1757.
21. J. Solà, Int. J. of Mod. Phys. D**27** (2018) 1847029; J. de Cruz Pérez & J. Solà, Mod. Phys. Lett. A33 (2018) 1850228.
22. S.M. Turner & M. White, Phys. Rev. D**56** (1997) R4439.
23. P.J.E. Peebles & B. Ratra, ApJ **325** (2018) L17; Phys. Rev. D**37** (1988) 3406.
24. E.D. Valentino, A. Melchiorri & O. Mena, Phys. Rev. D**96** (2017) 043503.
25. S.M. Feeney *et al.,* Phys. Rev. Lett. **122** (2019) 061105; B.S. Haridasu, V.V. Luković, M. Moresco & N. Vittorio, JCAP **1810** (2018) 015; E. Macaulay *et al.* (DES Collab.), arXiv:1811.02376.
26. A. Gómez-Valent & L. Amendola, JCAP **1804** (2018) 051; A. Gómez-Valent, arXiv:1810.02278.
27. S. Anand, P. Chaubal, A. Mazumdar & S. Mohanty, JCAP **1711** (2017) 005.
28. R. An, C. Feng & B. Wang, JCAP **1802** (2018) 038.